brain sciences

MDPI

Article

Anatomical Variations of the Common Carotid Arteries and Neck Structures of the New Zealand White Rabbit and Their Implications for the Development of Preclinical Extracranial Aneurysm Models

Gwendoline Boillat [1,2,*], Tim Franssen [2], Stefan Wanderer [1,2], Jeannine Rey [1,2], Daniela Casoni [3], Lukas Andereggen [1,2], Serge Marbacher [1,2] and Basil E. Gruter [1,2,4]

[1] Department of Neurosurgery, Kantonsspital Aarau, 5001 Aarau, Switzerland
[2] Cerebrovascular Research Group, Department for BioMedical Research, University of Bern, 3010 Bern, Switzerland
[3] Experimental Surgery Facility, Department for Biomedical Research, Faculty of Medicine, University of Bern, 3010 Bern, Switzerland
[4] Institute of Neuroradiology, Department of Radiology, Kantonsspital Aarau, 5001 Aarau, Switzerland
* Correspondence: gwendoline.boillat@ksa.ch

Abstract: Background: Rabbit models involving neck arteries are of growing importance for the development of preclinical aneurysm models. An optimal understanding of the anatomy is primordial to allow the conception of models while minimizing mortality and morbidity. The aim of this study is to give reliable anatomical landmarks to allow a standardized approach to the neck vessels. Methods: We performed a necropsy on nine specimens from ongoing experimental studies. We measured the distance between the origins of the right and left common carotid artery (rCCA/lCCA) and between the rCCA and the manubrium sterni (MS). The structures at risk were described. Results: Female New Zealand White rabbits (NZWR) weighing 3.7 ± 0.3 kg and aged 25 ± 5 weeks were included. The rCCA origin was located 9.6 ± 1.2 mm laterally and 10.1 ± 3.3 mm caudally to the MS. In all specimens, the lCCA originated from the aortic arch, together with the brachiocephalic trunk (BCT), and 6.2 ± 3.1 mm proximally to the rCCA origin. The external and internal jugular veins, trachea and laryngeal nerve were the main structures at risk. Conclusions: The data help to localize both CCAs and their origin to guide surgical approaches with the manubrium sterni as a main landmark. Special attention has to be paid to the trachea, jugular veins and laryngeal nerves.

Keywords: aneurysm; animal model; New Zeeland White Rabbit; carotid arteries; anatomy

Citation: Boillat, G.; Franssen, T.; Wanderer, S.; Rey, J.; Casoni, D.; Andereggen, L.; Marbacher, S.; Gruter, B.E. Anatomical Variations of the Common Carotid Arteries and Neck Structures of the New Zealand White Rabbit and Their Implications for the Development of Preclinical Extracranial Aneurysm Models. *Brain Sci.* **2023**, *13*, 222. https://doi.org/10.3390/brainsci13020222

Academic Editor: Giovanni Grasso

Received: 20 December 2022
Revised: 20 January 2023
Accepted: 25 January 2023
Published: 28 January 2023

1. Introduction

Due to its availability and easy handling, the rabbit model has been widely established and well characterized for preclinical studies [1]. Its vascular anatomical, physiological and hemodynamical characteristics, close to humans, make it an ideal model for vascular pathologies and, more specifically, to study the pathophysiology and treatments of aneurysms [2–8]. The surgical creation of aneurysms is usually performed on rabbit neck arteries, which have a comparable diameter to the human brain's major arteries (such as the middle cerebral artery). Among the various existing models, the elastase-digested stump aneurysm, consisting of an endovascular application of the elastase enzyme at the origin of the right common carotid artery (rCCA) and the ligation of the artery, is probably the most common one [9–12]. However, the procedure can be associated with complications and additional mortality due to the presence of the aberrant origin of the tracheoesophageal branches and the superior thyroid artery from the proximal portion of the CCA [13]. In order to overcome this issue, research groups developed an open technique to expose the rCCA at its origin and surgically temporarily clip the vessel during the application of the

elastase solution and ligate the artery afterward [9,12]. Furthermore, complex aneurysm creation, such as bifurcation aneurysm models, always implies an open approach, including the dissection of the neck arteries and microsurgical anastomosis [14–16], where a good knowledge of anatomy is mandatory to avoid lesions of vital structures, such as the trachea, great vessels (arteries and veins) and nerves of the neck, as well as the pleura. However, the exact vascular anatomy of the rabbit is not well described, and previous radiological studies have suggested a high variability in the anatomical position of vascular structures [17,18]. Moreover, the region of the CCA's origin contains the above-mentioned vital structures, which can be at risk of damage during aneurysm creation surgeries.

The aims of this work are to describe reliable landmarks for the localization of the origin of the CCAs; to observe how the anatomical variation of the vessels may impact the surgical approach; and to describe which anatomical structures are at higher risk of damage during surgeries on the neck arteries.

2. Materials and Methods

2.1. Study Design and Animals

In this study, $n = 9$ cadavers of female New Zealand White (NZW) rabbits (Charles River Laboratories) weighing 3.7 kg ($\pm$360 g) and with a mean age of 25 $\pm$ 5 weeks were included. Specimens were received after euthanasia, performed in the setting of previous experimental series. The original studies were performed in accordance with the institutional guidelines for the care and use of experimental animals and following the ARRIVE guidelines. They were approved by the animal care committee of the Canton of Bern, Switzerland (approval number BE 108/16). Euthanasia was performed by intravenous injection of pentobarbital 120 mg/kg (Esconarkon ad us. vet., Streuli, Switzerland). Dissection and anatomical measures were performed immediately after euthanasia.

2.2. Approach and Measures

Each rabbit was dissected in the region of the neck from the larynx to approximately the third rib in order to expose the great vessels of the neck and the surrounding structures. After a median skin incision, the musculature of the neck was exposed and dissected. The sternocephalicus muscle (SCM) was reclined rostrally in order to expose the underlying vessels. The tissues around the CCAs were dissected to allow good visibility of the vascular structures and surrounding nerves. To access the region of the brachiocephalic trunk and the rCCA origin, the medial part of the first rib was removed. The brachiocephalic trunk (BCT), rCCA and left CCA (lCCA) were exposed to allow for measurements. The distance between the rCCA origin and manubrium tip (incisura jugularis) was measured in craniocaudal and mediolateral directions using a tape ruler and a measuring clip. In the same way, the distance between both rCCA and lCCA origins was recorded. Lastly, we identified both CCAs' origins and classified them into 3 variations, based on the previously described classification by Ding et al. [17]: Type 1: lCCA originating from the bifurcation of the aortic arch and the BCT; Type 2: lCCA originating from the aortic arch; Type 3: lCCA originating from the BCT itself, next to the rCCA (Figure 1).

2.3. Neck Dissection

In order to describe the relevant anatomical structures at risk during an approach to the rCCA, we performed a complete neck dissection. Each step was photographically documented and every structure was described, based on anatomical atlas references [19,20]. First, a median skin incision was performed from the manubrium tip to the hyoid bone. The fat pad was removed in order to expose the superficial musculature (Figure 2A). The descending pectoral muscle (DPM) (Figure 2B), first rib and tip of the manubrium were removed to allow access to the caudal part of the great vessels (Figure 2C). Meticulous soft tissue dissection around the vascular and neural structures was performed in order to follow the courses of the structures. Both sternocephalicus muscles (SCMs) were cranially reclined to access the deep musculature (Figure 2D), and finally, the sternothyroid muscle

(STM), running above the trachea, was cranially reclined, and pericardial fat was exposed (Figure 2E). Pericardial fat was finally removed to expose the heart and the origin of the great vessels (Figure 2F). The structures identified to be at risk during the approach to the neck vessels were defined as structures in direct contact with the carotid arteries or structures that have to be strongly manipulated during the approach. These were documented in detail.

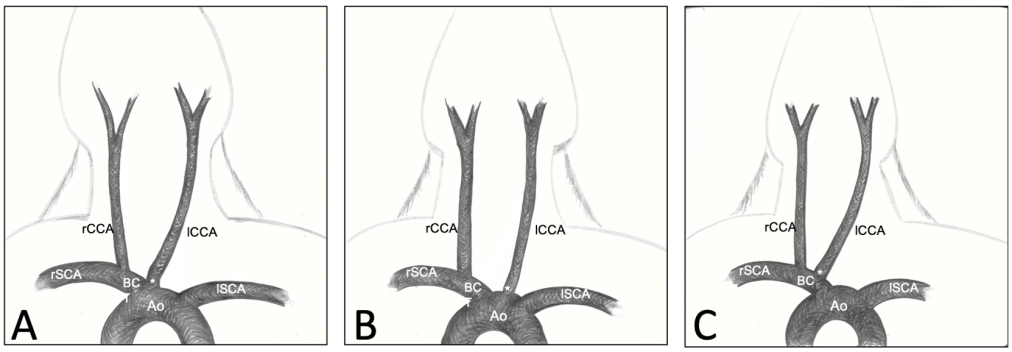

Figure 1. Classification of the three CCAs' origin variations. Type 1: lCCA originating from the bifurcation of the aortic arch and the BCT (**A**); Type 2: lCCA originating from the aortic arch (**B**); Type 3: lCCA originating from the BCT, next to the rCCA (**C**).

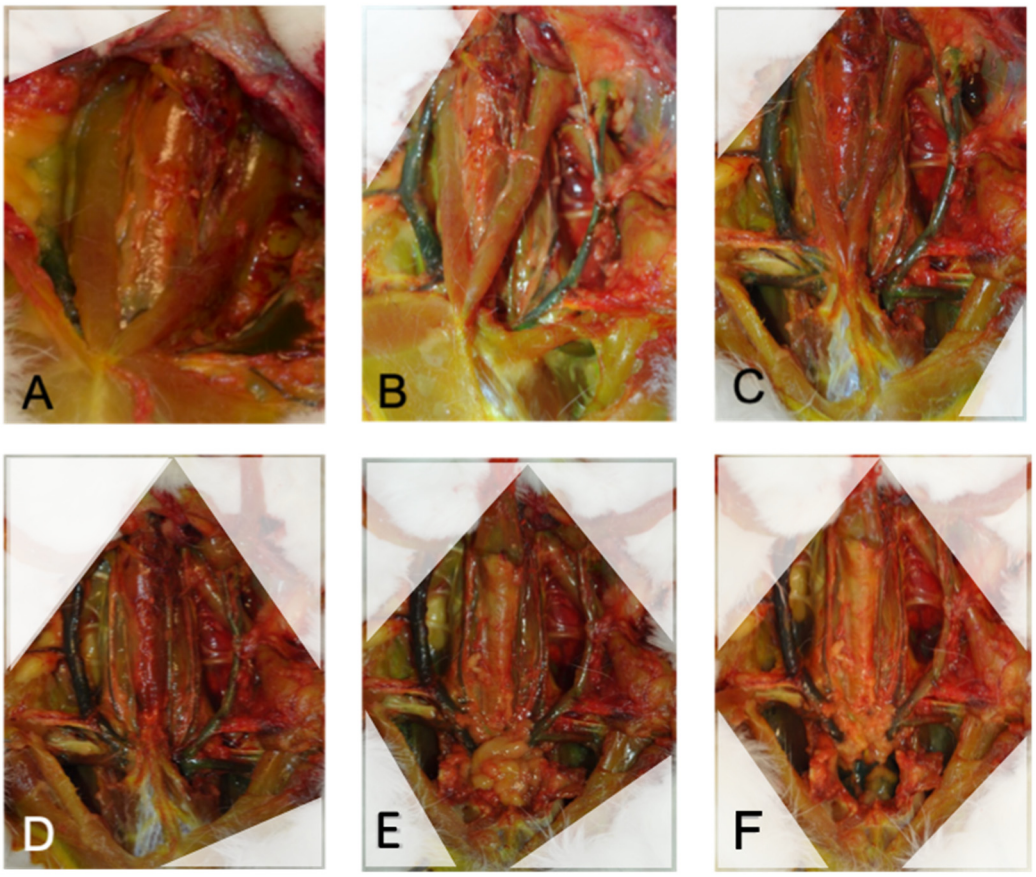

Figure 2. Illustration of the dissection step by step. (**A**) After median skin incision and fat pad resection. (**B**) After removal of the lDPM and first rib on the left side. (**C**) After removal of the rDPM and first rib on the right side. (**D**) After section and reclination of both SCM. (**E**) After section and reclination of the STM. (**F**) After dissection of the heart cavity. Note the reclined SCM/STM in the white triangles in (**D**–**F**).

3. Results

The tip of the manubrium sterni is a reliable landmark to guide dissection and find the origin of the rCCA, which should be located about 1 cm laterally and 1 cm caudally to it. The sternocephalicus muscle is a good landmark to find and follow the course of the CCAs on both sides of the trachea. During dissection, special attention should be paid to the jugular veins, the laryngeal nerves and the trachea itself.

3.1. Distance between rCCA's Origin, Manubrium and lCCA's Origin

The mean distance between the origin of the rCCA at the BCT and the tip of the manubrium in the mediolateral direction was 9.6 mm ±1.2 mm. In the craniocaudal direction, the mean distance was 10.1 mm ±3.3 mm. Detailed data are shown in Table 1 and Figure 3. The mean distance separating the origin of the rCCA and the lCCA was 6.2 mm ±3.1 mm. Detailed data are shown in Table 2 and Figure 3.

Table 1. Measured distance between the tip of the manubrium and the origin of the right common carotid artery at the brachiocephalic trunk in a mediolateral direction (SD ± 1.2 mm) and a craniocaudal direction (SD ± 3.3 mm).

Animal Number	Mediolateral Direction (mm)	Craniocaudal Direction (mm)
1	10	8
2	10	7
3	10	10
4	10	8
5	8	6
6	12	15
7	9	12
8	9	15
9	8	10
Mean (±SD)	9.6 (±1.2)	10.1 (±3.3)

Table 2. Measured distance between both origins of the common carotid arteries (SD ± 3.1 mm).

Animal Number	Distance (mm)
1	4
2	4
3	6
4	4
5	12
6	4
7	8
8	4
9	10
Mean (±SD)	6.2 (±3.1)

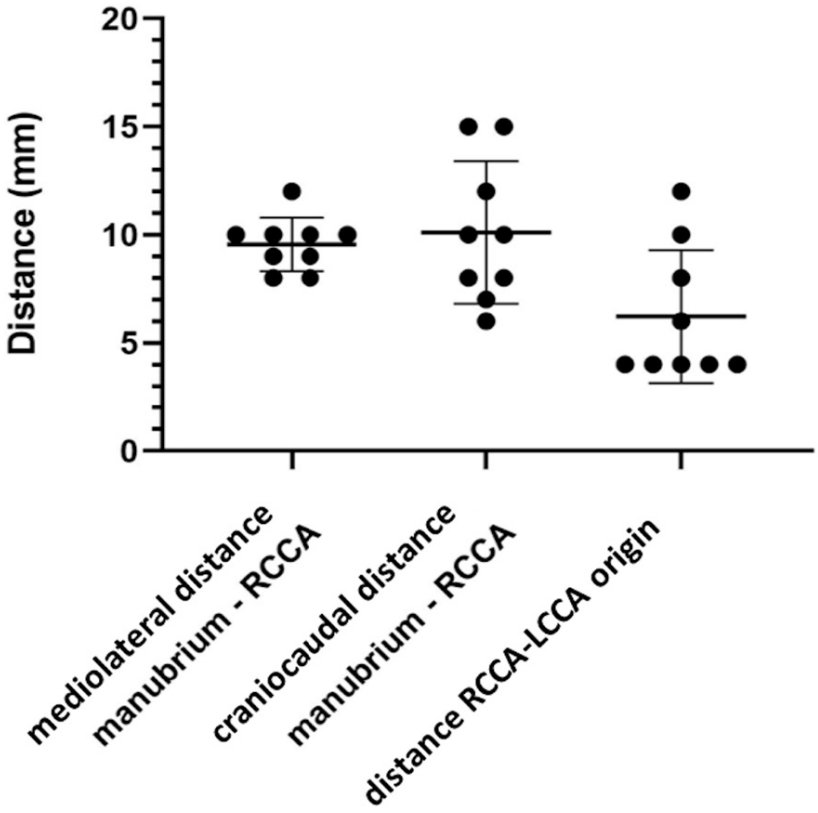

Figure 3. Measured distance between the tip of the manubrium and the origin of the right common carotid artery at the brachiocephalic trunk in a mediolateral direction (SD ± 1.2 mm), in the craniocaudal direction (SD ± 3.3 mm) and distance between RCCA and LCCA origins (SD ± 3.1 mm).

3.2. Variations of CCA's Origin

In all nine animals (100%), the rCCA originated from the BCT, and the lCCA originated from the bifurcation of the BCT and the aortic arch, corresponding to the Type 1 variation. No rabbits showed Types 2 or 3 vessel locations with lCCA directly originating from the aortic arch or lCCA originating next to the rCCA from the BCT. We also did not observe the aberrant variation of the subclavian artery (SCA) anatomy (Figure 1).

3.3. Descriptive Anatomy

After skin incision and subcutaneous fat tissue dissection, the first layer of muscles inserting on the manubrium sterni becomes visible: first, the sternocephalicus muscle (SCM) and then, medially to it and laying above the trachea, the sternothyroid (STM) and the sternohyoid muscles (SHMs). The transverse/descending pectoral muscles (TPM/DPM) find their origin at the manubrium sterni and insert laterally in the crista humeri (Figure 4A). The SCM covers the CCAs and the internal jugular veins (IJVs) on both sides of the trachea and has to be dissected and reclined to access the vessels. Cranially, the CCAs run medially to the SCM, whereas caudally, they run more laterally (Figure 4C). Under the SCM and laterally to the STM and SHM run the CCAs, the vagal nerve and the IJV. The three structures are bounded together with connective tissue. Cranially, these connective tissues are rather loose, and the distance between the artery and vein measures about 5–10 mm. However, caudally, the EJV comes medially in contact with the artery, and the nerve crosses in between. This makes a dissection more difficult in the caudal area (Figures 4D and 5). In most cases, a transversal jugular vein can be seen at the level of the manubrium sterni and limits further dissection caudally. The vein is an anastomosis between both EJVs and can be cut in the middle to allow access to the caudal portion of the great vessels (Figure 4B). Further, caudally, the rCCA runs under the clavicle and comes above the trachea to join the

rSCA at the BCT. Laterally, the vagal nerve (VN) crosses above the SCA and the EJV and IJV and meets the right subclavian vein (rSCV). The BCT meets the aortic arch and both aorta and SCV join the heart. The thymus can be observed superficially covering this part of the vessels. On the left side, the lCCA crosses above the trachea to join the origin of the BCT on the aortic arch. Figure 5 gives an overview of the deep neurovascular structures after the resection of the muscular and bony layers.

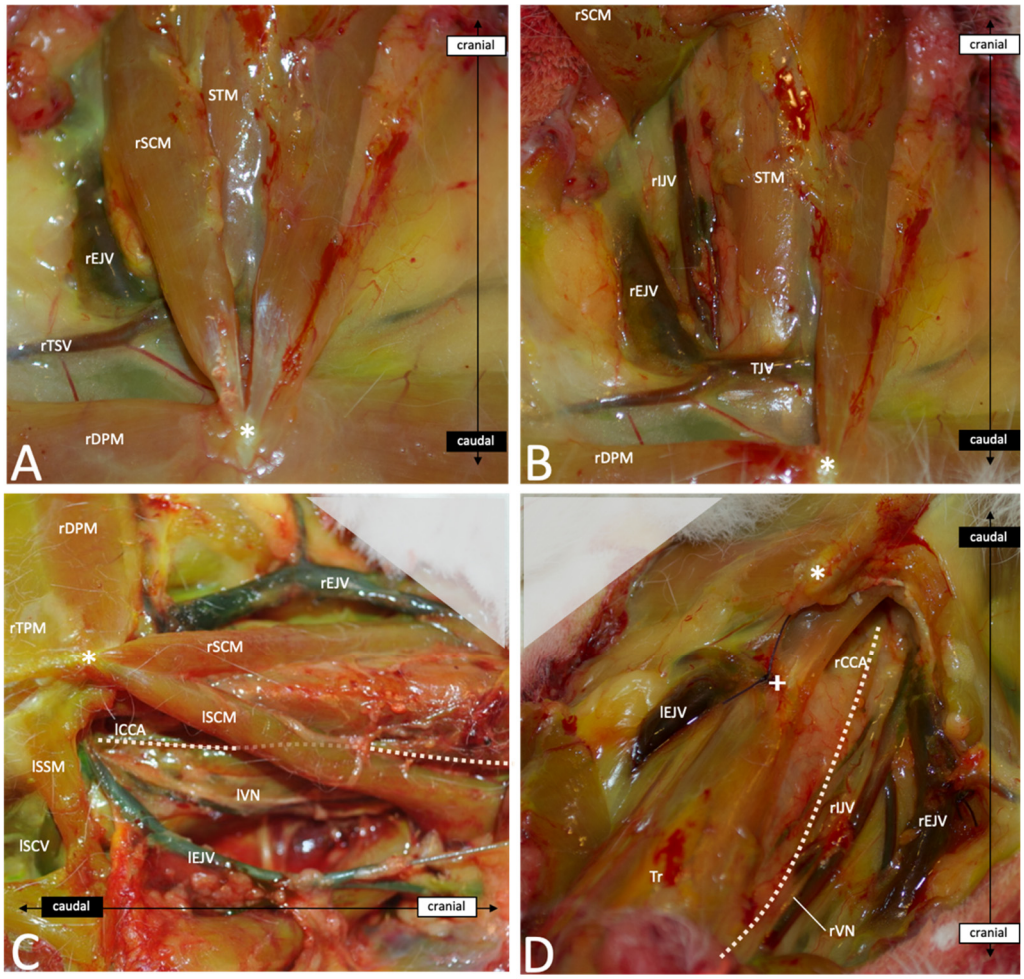

Figure 4. (**A**) Frontal view of the first superficial layer after skin incision and subcutaneous fat tissue dissection. (**B**) Frontal view after proximal section and reclination of the rSCM on the right side. (**C**) Left lateral view (surgical view for the approach on the left side of the neck) after resection of the lDMP and lTPM and dissection of the connective and fat tissue to free the neurovascular structures. The dotted line highlights the course of lCCA. (**D**) Cranial oblique overview on the right side (surgical view for the approach on the rCCA) after resection of the SCMs, the rDPM and rTPM and section of the TJV. The dotted line highlights the course of the rCCA. Abbreviations: *—tip of the manubrium sterni; +—section point of the transversal jugular vein; Tr—trachea; rSCM—right sternocephalicus muscle; lSCM—left sternocephalicus muscle; STM—sternothyroid muscle; rDPM—right descending pectoral muscle; rTPM—right transverse pectoral muscle; lSSM—left sternoscapular muscle; rEJV—right external jugular vein; lEJV—left external jugular vein; rIJV—right internal jugular vein; lIJV—left internal jugular vein; rTSV—right transverse scapular vein; TJV—transversal jugular vein; lSCV—left subclavian vein; lCCA—left common carotid artery; rCCA—right common carotid artery; lVN—left vagal nerve; rVN—right vagal nerve.

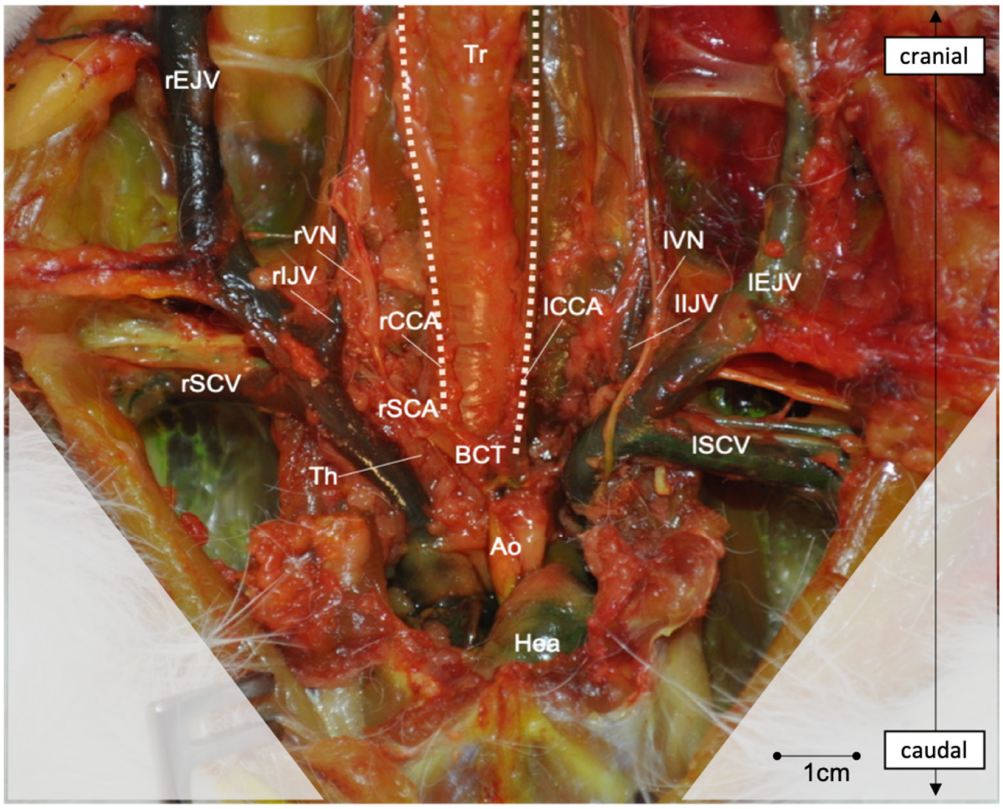

Figure 5. Frontal overview of the deep neurovascular structures of the neck after resection of the muscle layers and cranial part of the thoracic cage. SCM, STM, SHM, DPM, TPM, and SSM, as well as the clavicle, the three first ribs and the cranial third of manubrium sterni were removed. Subcutaneous fat, thymus and pericardial fat were dissected and removed to free the vessels and nerves. The dotted lines highlight the course of the rCCA and lCCA. Abbreviations: Tr—trachea; Hea—heart; Th—thymus; SCM—sternocephalicus muscle; STM—sternothyroid muscle; DPM—descending pectoral muscle; TPM—transverse pectoral muscle; SSM—sternoscapular muscle; rEJV—right external jugular vein; lEJV—left external jugular vein; rIJV—right internal jugular vein; lIJV—left internal jugular vein; rSCV—right subclavian vein; lSCV—left subclavian vein; Ao—aorta; BCT—brachiocephalic trunk; lCCA—left common carotid artery; rCCA—right common carotid artery; lVN—left vagal nerve; rVN—right vagal nerve.

4. Discussion

The rabbit aneurysm model is of great interest for the study and better understanding of the pathophysiological aspects of human intracranial aneurysms [4,5,7,21–27]. Scientists are constantly developing new models or refining the existing models for the creation of aneurysms on rabbit neck arteries [5–7,9,11,14,16,28–32]. The elastase-induced aneurysm model is one of the most commonly used and well described [28,29,33–37] and is widely used for endovascular device testing [38–48]. However, in a previous series, the periprocedural mortality of the rabbit elastase model was reported at around 8% [49,50]. Given the number of studies that conceal complications and mortality rates, this number could be even higher. For instance, research investigating the morbidity of the model showed complication rates reaching >50% [49–52]. As morbidity and mortality could influence the quality of the scientific result [53], and given the growing importance of animal welfare in preclinical studies, the impact of complications must not be underestimated and should be a concern for every scientist.

If the age and weight of the animal, as well as the duration of the procedure, have been demonstrated to be determinizing factors for postoperative complications, the direct injury of the structures of the neck through endovascular or surgical procedures are recognized to

be a critical source of failure. In order to efficiently improve the techniques, avoid pitfalls and develop new approaches with lower morbidity and mortality, the clinician and/or scientist have to acquire sufficient knowledge of the anatomy of the animal. Unfortunately, the current literature and even the veterinary educational resources lack exact information about detailed anatomy and its possible variations, particularly in the region of the neck. This study gives anatomical reliable landmarks to allow a standardized approach to the neck vessels, with low morbidity and mortality. This study shows that in order to expose the origin of the rCCA, the manubrium sterni can be used to guide the dissection, which should be performed about 1 cm laterally and caudally to the incisura jugularis. There are no relevant variations to expect between animals of the same breed and with similar ages, as we found only variability of a few millimeters between the rabbits. However, the distance between the rCCA and lCCA origins varied between 4 and 12 mm in this study. Thus, the origin of one CCA should not be used to guide the dissection of the second one, and dissection from cranial to caudal is recommended to find the origin of the CCAs. Instead, the SCM can be used to find and follow the CCAs, which run laterally to the caudal part of the muscle and medially to its cranial part. As the muscle plays a key role in head motion, especially rotation and inclination, lesions have to be avoided during dissection, and smooth instruments such as anatomical forceps and vessel loops are of great help for this step of the surgery. Furthermore, the SCM runs laterally to the external jugular vein (EJV), which is at risk of injury while dissecting the lateral part of the muscle. A wet swab provides good protection against sharp instrument manipulation and prevents dryness and weakening of the wall.

On the other hand, Ding et al. already focused on the possible variations concerning the carotid arteries that may impact endovascular approaches in the elastase model [17]. The authors found three main variations of the carotid origins (Figure 1) that can impact catheterizing as well as open surgery. In the present study, both CCAs originate from the BCT according to the Type 1 variation described by Ding et al., with the rCCA originating from the BCT and the lCCA originating from the bifurcation of the BCT and aortic arch. This is also consistent with most of the data shown in the anatomical atlas references [19,20]. Variations of these origins or other uncommon variant arteries may, however, significantly affect the surgery and even impact the testing of endovascular techniques in an aneurysm model. Although rare, these variations have, thus, to be known and taken into consideration while working with such models. Furthermore, some authors experimented with dramatic tracheal necrosis and hemorrhage after endovascular elastase application in order to create an aneurysm [13,52,54], revealing the presence of aberrant superior thyroid arteries or anastomosis from the carotid arteries. This complication can be avoided by proceeding with open procedures, which allows the closure of the variant branches [9,12,33,55,56]. In order to perform safe interventions, anatomical landmarks and specific anatomical descriptions are definitely needed. Surgeons performing an approach to the great neck vessels have to pay special attention to numerous vital structures. The jugular veins, which run directly laterally to the rCCA and cross the right subclavian artery to form the rSCV, are at high risk of damage during the dissection of the proximal part of the CCAs. At the level of the rCCA origin from the BCT, the EJV comes directly in contact with the artery and may be adherent with it. The dissection has to be performed carefully on the side of the artery in order to avoid any damage to the venous wall. Such injuries are often untreatable and may result in the death of the animal. A different, important structure is the vagal nerve, including its laryngeal branches, which run directly with the CCAs and sometimes form the nervous plexus, which can be easily damaged by dissecting the vessels. Such injuries may lead to laryngeal paresis, which appears clinically as postoperative stridor and increases inspiratory effort. According to the severity of the damage, this can elevate intrapulmonary negative pressure with consecutive pulmonary edema, respiratory depression and death. Moreover, as illustrated in our study, the CCAs run along both sides of the trachea and cross above it to join the BCT and aortic arch. The trachea is a rather strong structure. However, direct pressure or traction during the dissection should be avoided in order to ensure

correct ventilation during the surgery, and the surgeon should pay attention not to injure the tracheal wall using sharp instruments during the approach. Lastly, the thymus lays just above the proximal rCCA and BCT and may obstruct the dissection of the proximal part of the CCA. So far, injury of the thymus has not been described as a mortal lesion, and it does not seem to cause any relevant morbidities in the postoperative phase. However, swelling and bleeding due to rough manipulation can significantly complicate the dissection, and we recommend preserving the gland as long as possible with the application of a wet swab.

The presented comprehensive overview should help surgeons to plan their operation and to minimize perioperative morbidity and mortality. In the same way, it is supposed to improve scientific results and support the development of further, sophisticated aneurysm models.

5. Conclusions

Our study demonstrates the tip of the manubrium sterni being a reliable landmark to guide dissection and find the origin of the rCCA, which should be located about 1 cm laterally and 1 cm caudally to it. The sternocephalicus muscle also helps to find and follow the course of the CCAs on both sides. Great variations of the CCAs' origin are rare within the NZW rabbit strain, and the insights into the specific anatomy of the neck provided in this study should help surgeons to avoid complications and improve surgical and scientific results.

Author Contributions: G.B.: conceptualization, methodology, data processing, formal analysis, writing the original draft, the creation of illustrations, reviewing and editing. T.F.: methodology, data processing, writing the original draft, illustrations and reviewing. S.W.: reviewing and editing. J.R.: reviewing and editing. D.C.: resources, reviewing and editing. L.A.: supervision, validation, reviewing and editing. S.M.: conceptualization, resources, funding acquisition, supervision, reviewing and editing. B.E.G.: conceptualization, methodology, data processing, formal analysis, supervision, validation, reviewing and editing. All authors have read and agreed to the published version of the manuscript.

Funding: This research did not receive specific grants from funding agencies in the public, commercial or nonprofit sectors. The initial research from which the specimens were taken was funded by a grant from the Swiss National Science Foundation (310030_182450/1).

Institutional Review Board Statement: The study was performed in accordance with institutional guidelines for the care and use of experimental animals and following the ARRIVE guidelines. They were approved by the animal care committee of the Canton of Bern, Switzerland (approval number BE 108/16).

Informed Consent Statement: Not applicable.

Data Availability Statement: The data presented in this study are available on request from the corresponding author.

Conflicts of Interest: The authors declare no conflict of interest.

References

1. Mapara, M.; Thomas, B.S.; Bhat, K.M. Rabbit as an animal model for experimental research. *Dent. Res. J.* **2012**, *9*, 111–118. [CrossRef]
2. Marbacher, S.; Strange, F.; Frosen, J.; Fandino, J. Preclinical extracranial aneurysm models for the study and treatment of brain aneurysms: A systematic review. *J. Cereb. Blood Flow Metab.* **2020**, *40*, 922–938. [CrossRef] [PubMed]
3. Thompson, J.W.; Elwardany, O.; McCarthy, D.J.; Sheinberg, D.L.; Alvarez, C.M.; Nada, A.; Snelling, B.M.; Chen, S.H.; Sur, S.; Starke, R.M. In vivo cerebral aneurysm models. *Neurosurg. Focus* **2019**, *47*, E20. [CrossRef]
4. Bouzeghrane, F.; Naggara, O.; Kallmes, D.; Berenstein, A.; Raymond, J.; The International Consortium of Neuroendovascular Centres. In Vivo Experimental Intracranial Aneurysm Models: A Systematic Review. *AJNR Am. J. Neuroradiol.* **2010**, *31*, 418–423. [CrossRef] [PubMed]
5. Short, J.G.; Fujiwara, N.H.; Marx, W.F.; Helm, G.A.; Cloft, H.J.; Kallmes, D.F. Elastase-Induced Saccular Aneurysms in Rabbits: Comparison of Geometric Features with Those of Human Aneurysms. *Am. J. Neuroradiol.* **2001**, *22*, 1833–1837. [PubMed]

6. Brinjikji, W.; Ding, Y.H.; Kallmes, D.F.; Kadirvel, R. From bench to bedside: Utility of the rabbit elastase aneurysm model in preclinical studies of intracranial aneurysm treatment. *J. NeuroInterv. Surg.* **2016**, *8*, 521–525. [CrossRef] [PubMed]
7. Zeng, Z.; Kallmes, D.F.; Durka, M.J.; Ding, Y.; Lewis, D.; Kadirvel, R.; Robertson, A.M. Hemodynamics and Anatomy of Elastase-Induced Rabbit Aneurysm Models: Similarity to Human Cerebral Aneurysms? *Am. J. Neuroradiol.* **2011**, *32*, 595–601. [CrossRef] [PubMed]
8. Konczalla, J.; Wanderer, S.; Mrosek, J.; Gueresir, E.; Schuss, P.; Platz, J.; Seifert, V.; Vatter, H. Levosimendan, a new therapeutic approach to prevent delayed cerebral vasospasm after subarachnoid hemorrhage? *Acta Neurochir.* **2016**, *158*, 2075–2083. [CrossRef] [PubMed]
9. Hoh, B.L.; Rabinov, J.D.; Pryor, J.C.; Ogilvy, C.S. A modified technique for using elastase to create saccular aneurysms in animals that histologically and hemodynamically resemble aneurysms in human. *Acta Neurochir.* **2004**, *146*, 705–711. [CrossRef] [PubMed]
10. Altes, T.A.; Cloft, H.J.; Short, J.G.; DeGast, A.; Do, H.M.; Helm, G.A.; Kallmes, D.F. Creation of Saccular Aneurysms in the Rabbit: A model suitable for testing endovascular devices. *Am. J. Roentgenol.* **2000**, *174*, 349–354. [CrossRef]
11. Krings, T.; Moller-Hartmann, W.; Hans, F.-J.; Thiex, R.; Brunn, A.; Scherer, K.; Meetz, A.; Dreeskamp, H.; Stein, K.-P.; Gilsbach, J.M.; et al. A refined method for creating saccular aneurysms in the rabbit. *Neuroradiology* **2003**, *45*, 423–429. [CrossRef] [PubMed]
12. Ding, Y.H.; Danielson, M.A.; Kadirvel, R.; Dai, D.; Lewis, D.A.; Cloft, H.J.; Kallmes, D.F. Modified technique to create morphologically reproducible elastase-induced aneurysms in rabbits. *Neuroradiology* **2006**, *48*, 528–532. [CrossRef]
13. Möller-Hartmann, W.; Krings, T.; Stein, K.P.; Dreeskamp, A.; Meetz, A.; Thiex, R.; Hans, F.J.; Gilsbach, J.M.; Thron, A. Aberrant Origin of the Superior Thyroid Artery and the Tracheoesophageal Branch from the Common Carotid Artery: A Source of Failure in Elastase-Induced Aneurysms in Rabbits. *Am. J. Roentgenol.* **2003**, *181*, 739–741. [CrossRef] [PubMed]
14. Wanderer, S.; Waltenspuel, C.; Grüter, B.E.; Strange, F.; Sivanrupan, S.; Remonda, L.; Widmer, H.R.; Casoni, D.; Andereggen, L.; Fandino, J.; et al. Arterial Pouch Microsurgical Bifurcation Aneurysm Model in the Rabbit. *J. Vis. Exp.* **2020**, *159*, e61157. [CrossRef]
15. Marbacher, S.; Erhardt, S.; Schläppi, J.-A.; Coluccia, D.; Remonda, L.; Fandino, J.; Sherif, C. Complex Bilobular, Bisaccular, and Broad-Neck Microsurgical Aneurysm Formation in the Rabbit Bifurcation Model for the Study of Upcoming Endovascular Techniques. *Am. J. Neuroradiol.* **2011**, *32*, 772–777. [CrossRef] [PubMed]
16. Sherif, C.; Fandino, J.; Erhardt, S.; Di Ieva, A.; Killer, M.; Kleinpeter, G.; Marbacher, S. Microsurgical Venous Pouch Arterial-Bifurcation Aneurysms in the Rabbit Model: Technical Aspects. *J. Vis. Exp.* **2011**, *51*, 2718. [CrossRef]
17. Ding, Y.H.; Dai, D.; Layton, K.F.; Lewis, D.A.; Danielson, M.A.; Kadirvel, R.; Cloft, H.J.; Kallmes, D.F. Vascular Anatomic Variation in Rabbits. *J. Vasc. Interv. Radiol.* **2006**, *17*, 1031–1035. [CrossRef]
18. Lee, J.S.; Hamilton, M.G.; Zabramski, J.M. Variations in the anatomy of the rabbit cervical carotid artery. *Stroke* **1994**, *25*, 501–503. [CrossRef]
19. Popesko, P.; Rajtová, V.; Horák, J.i. *A Colour Atlas of the Anatomy of Small Laboratory Animals*; Wolfe Pub. Ltd.: London, UK, 1992.
20. Barone, R. *Atlas of Rabbit Anatomy*; Masson: Paris, France, 1973; p. 219.
21. Abruzzo, T.; Shengelaia, G.G.; Dawson, R.C.; Owens, D.S.; Cawley, C.M.; Gravanis, M.B. Histologic and morphologic comparison of experimental aneurysms with human intracranial aneurysms. *Am. J. Neuroradiol.* **1998**, *19*, 1309–1314.
22. Aoki, T.; Nishimura, M. The Development and the Use of Experimental Animal Models to Study the Underlying Mechanisms of CA Formation. *J. Biomed. Biotechnol.* **2011**, *2011*, 535921. [CrossRef]
23. Dai, D.; Ding, Y.H.; Danielson, M.A.; Kadirvel, R.; Lewis, D.A.; Cloft, H.J.; Kallmes, D.F. Histopathologic and Immunohistochemical Comparison of Human, Rabbit, and Swine Aneurysms Embolized with Platinum Coils. *Am. J. Neuroradiol.* **2005**, *26*, 2560–2568. [PubMed]
24. Zaragoza, C.; Gomez-Guerrero, C.; Martin-Ventura, J.L.; Blanco-Colio, L.M.; Lavin, B.; Mallavia, B.; Tarin, C.; Mas, S.; Ortiz, A.; Egido, J. Animal Models of Cardiovascular Diseases. *J. Biomed. Biotechnol.* **2011**, *2011*, 497841. [CrossRef] [PubMed]
25. Frösen, J.; Piippo, A.; Paetau, A.; Kangasniemi, M.; Niemelä, M.; Hernesniemi, J.; Jääskeläinen, J. Remodeling of Saccular Cerebral Artery Aneurysm Wall Is Associated with Rupture: Histological analysis of 24 unruptured and 42 ruptured cases. *Stroke* **2004**, *35*, 2287–2293. [CrossRef]
26. Frösen, J.; Piippo, A.; Paetau, A.; Kangasniemi, M.; Niemelä, M.; Hernesniemi, J.; Jääskeläinen, J. Growth Factor Receptor Expression and Remodeling of Saccular Cerebral Artery Aneurysm Walls: Implications for Biological Therapy Preventing Rupture. *Neurosurgery* **2006**, *58*, 534–541. [CrossRef] [PubMed]
27. Stehbens, W.E. In re: Histologic and morphologic comparison of experimental aneurysms with human intracranial aneurysms. *Am. J. Neuroradiol.* **2000**, *21*, 1770.
28. Ding, Y.; Dai, D.; Lewis, D.; Danielson, M.; Kadirvel, R.; Cloft, H.; Kallmes, D. Long-Term Patency of Elastase-Induced Aneurysm Model in Rabbits. *Am. J. Neuroradiol.* **2006**, *27*, 139–141. [PubMed]
29. Marbacher, S.; Tastan, I.; Neuschmelting, V.; Erhardt, S.; Coluccia, D.; Sherif, C.; Remonda, L.; Fandino, J. Long-term patency of complex bilobular, bisaccular, and broad-neck aneurysms in the rabbit microsurgical venous pouch bifurcation model. *Neurol. Res.* **2012**, *34*, 538–546. [CrossRef] [PubMed]
30. Sherif, C.; Marbacher, S.; Erhardt, S.; Fandino, J. Improved Microsurgical Creation of Venous Pouch Arterial Bifurcation Aneurysms in Rabbits. *Am. J. Neuroradiol.* **2011**, *32*, 165–169. [CrossRef] [PubMed]
31. Sherif, C.; Marbacher, S.; Fandino, J. High-resolution three-dimensional 3 T magnetic resonance angiography for the evaluation of experimental aneurysm in the rabbit. *Neurol. Res.* **2009**, *31*, 869–872. [CrossRef] [PubMed]

32. Strange, F.; Grüter, B.E.; Fandino, J.; Marbacher, S. Preclinical Intracranial Aneurysm Models: A Systematic Review. *Brain Sci.* **2020**, *10*, 134. [CrossRef] [PubMed]
33. Origuchi, N.; Shigematsu, H.; Izumiyama, N.; Nakamura, K.; Toku, A.; Muto, T. Aneurysm induced by periarterial application of elastase heals spontaneously. *Int. Angiol.* **1998**, *17*, 113–119. [PubMed]
34. Ho, J.P.; Galex, I.A.; Sadeghi, N.B.; Weledji, N.; Bermudez, S.I.C.; Mitchell, B.A.; Bush, D.M.; Yap, E.; Davis, N.C.; Catalino, M.P.; et al. Rabbit Elastase Aneurysm: Imaging and Histology Correlates for Inflammation and Healing. *World Neurosurg.* **2021**, *148*, e242–e251. [CrossRef]
35. Sasaki, K.; Ujiie, H.; Higa, T.; Hori, T.; Shinya, N.; Uchida, T. Rabbit Aneurysm Model Mediated by the Application of Elastase. *Neurol. Med. Chir.* **2004**, *44*, 467–474. [CrossRef] [PubMed]
36. Seong, J.; Sadasivan, C.; Onizuka, M.; Gounis, M.J.; Christian, F.; Miskolczi, L.; Wakhloo, A.K.; Lieber, B.B. Morphology of elastase-induced cerebral aneurysm model in rabbit and rapid prototyping of elastomeric transparent replicas. *Biorheology* **2005**, *42*, 345–361.
37. Thiex, R.; Hans, F.J.; Scherer, K.; Krings, T.; Möller-Hartmann, W. Are the configuration and neck morphology of experimental aneurysms predictable? A technical approach. *Neuroradiology* **2004**, *46*, 571–576. [CrossRef]
38. Killer, M.; Kallmes, D.; Jones, R.; Ding, Y.; Vestal, M.; Hauser, T.; Virmani, R.; Cruise, G. Long-Term Angiographic and Histological Results of a New Hydrogel-Containing Filling Coil in Experimental Rabbit Aneurysms. *Min Minim. Invasive Neurosurg.* **2010**, *53*, 97–105. [CrossRef] [PubMed]
39. Killer, M.; Kallmes, D.F.; McCoy, M.R.; Ding, Y.-H.; Shum, J.C.; Cruise, G.M. Angiographic and Histologic Comparison of Experimental Aneurysms Embolized with Hydrogel Filaments. *Am. J. Neuroradiol.* **2009**, *30*, 1488–1495. [CrossRef]
40. Struffert, T.; Lang, S.; Adamek, E.; Engelhorn, T.; Strother, C.M.; Doerfler, A. Angiographic C-arm CT visualization of the Woven EndoBridge Cerebral Aneurysm Embolization Device (WEB): First Experience in an Animal Aneurysm Model. *Clin. Neuroradiol.* **2014**, *24*, 43–49. [CrossRef]
41. Struffert, T.; Roth, C.; Romeike, B.; Grunwald, I.O.; Reith, W. Onyx in an experimental aneurysm model: Histological and angiographic results. *J. Neurosurg.* **2008**, *109*, 77–82. [CrossRef]
42. Bai, Y.; Ding, X.; Zhao, Q.; Sun, H.; Li, T.; Li, Z.; Wang, H.; Zhang, L.; Zhang, C.; Xu, S. Development of an organic acid compound disinfectant to control food-borne pathogens and its application in chicken slaughterhouses. *Poult. Sci.* **2022**, *101*, 101842. [CrossRef]
43. Wang, K.; Yuan, S.; Zhang, X.; Liu, Q.; Zhong, Q.; Zhang, R.; Lu, P.; Li, J. Biodegradable flow-diverting device for the treatment of intracranial aneurysm: Short-term results of a rabbit experiment. *Neuroradiology* **2013**, *55*, 621–628. [CrossRef] [PubMed]
44. Chavan, R.; Pons, S.; Gupta, V.; Hui, D.; Bose, A. Safety and performance of the Penumbra Liberty stent system in a rabbit aneurysm model. *J. NeuroInterv. Surg.* **2015**, *7*, 266–271. [CrossRef] [PubMed]
45. Nishi, S.; Nakayama, Y.; Ishibashi-Ueda, H.; Yoshida, M.; Yonetani, H. Treatment of rabbit carotid aneurysms by hybrid stents (microporous thin polyurethane-covered stents): Preservation of side-branches. *J. Biomater. Appl.* **2014**, *28*, 1097–1104. [CrossRef] [PubMed]
46. Nishi, H.; Ishii, A.; Ono, I.; Abekura, Y.; Ikeda, H.; Arai, D.; Yamao, Y.; Okawa, M.; Kikuchi, T.; Nakakura, A.; et al. Biodegradable Flow Diverter for the Treatment of Intracranial Aneurysms: A Pilot Study Using a Rabbit Aneurysm Model. *J. Am. Heart Assoc.* **2019**, *8*, e014074. [CrossRef]
47. Grunwald, I.Q.; Romeike, B.; Eymann, R.; Roth, C.; Struffert, T.; Reith, W. An Experimental Aneurysm Model: A Training Model for Neurointerventionalists. *Interv. Neuroradiol.* **2006**, *12*, 17–24. [CrossRef]
48. Tsumoto, T.; Terada, T.; Yamaga, H.; Itakura, T. Coil Embolization Training Using a Rabbit Saccular Aneurysm Model. *Interv. Neuroradiol.* **2006**, *12*, 57–60. [CrossRef]
49. Lewis, D.A.; Ding, Y.H.; Dai, D.; Kadirvel, R.; Danielson, M.A.; Cloft, H.J.; Kallmes, D.F. Morbidity and Mortality Associated with Creation of Elastase-Induced Saccular Aneurysms in a Rabbit Model. *Am. J. Neuroradiol.* **2009**, *30*, 91–94. [CrossRef]
50. Cesar, L.; Miskolczi, L.; Lieber, B.B.; Sadasivan, C.; Gounis, M.J.; Wakhloo, A.K. Neurological deficits associated with the elastase-induced aneurysm model in rabbits. *Neurol. Res.* **2009**, *31*, 414–419. [CrossRef]
51. Villano, J.S.; Boehm, C.A.; Carney, E.L.; Cooper, T.K. Complications of elastase-induced arterial saccular aneurysm in rabbits: Case reports and literature review. *Comp. Med.* **2012**, *62*, 480–486.
52. Wang, K.; Huang, Q.; Hong, B.; Xu, Y.; Zhao, W.; Chen, J.; Zhao, R.; Liu, J. Neck Injury Is Critical to Elastase-Induced Aneurysm Model. *Am. J. Neuroradiol.* **2009**, *30*, 1685–1687. [CrossRef]
53. Grüter, B.E.; Croci, D.; Schöpf, S.; Nevzati, E.; D'Allonzo, D.; Lattmann, J.; Roth, T.; Bircher, B.; Muroi, C.; Dutilh, G.; et al. Systematic Review and Meta-analysis of Methodological Quality in In Vivo Animal Studies of Subarachnoid Hemorrhage. *Transl. Stroke Res.* **2020**, *11*, 1175–1184. [CrossRef] [PubMed]
54. Brunn, A.; Scherer, K.; Gilsbach, J.M.; Thron, A.; Krings, T.; Thiex, R.; Hans, F.J.; Möller-Hartmann, W. Haemorrhagic tracheal necrosis as a lethal complication of an aneurysm model in rabbits via endoluminal incubation with elastase. *Acta Neurochir.* **2004**, *146*, 285–289. [CrossRef]

55. Boillat, G.; Franssen, T.; Grüter, B.; Wanderer, S.; Catalano, K.; Casoni, D.; Andereggen, L.; Marbacher, S. Creation of Two Saccular Elastase-digested Aneurysms with Different Hemodynamics in One Rabbit. *J. Vis. Exp.* **2021**, e62518. [CrossRef]
56. Ding, Y.H.; Dai, D.; Danielson, M.A.; Kadirvel, R.; Lewis, D.A.; Cloft, H.J.; Kallmes, D.F. Control of Aneurysm Volume by Adjusting the Position of Ligation During Creation of Elastase-Induced Aneurysms: A Prospective Study. *Am. J. Neuroradiol.* **2007**, *28*, 857–859. [PubMed]